Chinese Chemical Letters 37 (2026) 111156

Contents lists available at ScienceDirect

Chinese Chemical Letters

journal homepage: www.elsevier.com/locate/cclet

Achieving superior sodium storage performance of brown coal-derived hard carbon by pre-oxidation

Ke Liu[a,1], Yujie Guo[a,b,1], Boyuan Liu[a,b], Yanjia Zhang[a,b], Yingjie Zhang[a,b], Xunzhu Zhou[c], Xingqiao Wu[c], Jie Xiao[a,b,*], Lin Li[c,*], Xiaoyuan Zeng[a,b,*]

[a] National and Local Joint Engineering Research Center for Lithium-ion Batteries and Materials Preparation Technology, Key Laboratory of Advanced Battery Materials of Yunnan Province, Faculty of Materials Science and Engineering, Kunming University of Science and Technology, Kunming 650093, China
[b] Faculty of Metallurgical and Energy Engineering, Kunming University of Science and Technology, Kunming 650093, China
[c] Institute for Carbon Neutralization Technology, College of Chemistry and Materials Engineering, Wenzhou University, Wenzhou 325035, China

ARTICLE INFO

Article history:
Received 5 February 2025
Revised 20 March 2025
Accepted 27 March 2025
Available online 27 March 2025

Keywords:
Sodium-ion batteries
Hard carbon
Brown coal
Pre-oxidation
Electrochemical performance

ABSTRACT

Hard carbon with abundant resources and superior sodium storage performance is the most representative anode material for sodium-ion batteries (SIBs), but suffers from unsatisfied reversible capacity and low initial Coulombic efficiency. Herein, brown coal is employed as the precursor to obtain high-performance hard carbon anode materials with the assistance of pre-oxidation treatment for SIBs. The unique pre-oxidation treatment introduces an abundance of oxygen-containing functional groups to regulate the microstructure of hard carbon anode, achieving a more disordered phase structure for improved sodium storage performance. These enable a high reversible specific capacity of 316.1 mAh/g with an initial Coulombic efficiency of 87.6%, significantly higher than those of 236.5 mAh/g and 71.7% in carbonized pristine brown coal. Meanwhile, the adsorption-insertion-pore filling sodium storage mechanism of brown coal-derived hard carbon is demonstrated by *in-situ* XRD and Raman. This work emphasizes the role of pre-oxidation treatment on boosting the sodium storage performance of brown coal-derived hard carbon for advanced SIBs.

© 2026 Published by Elsevier B.V. on behalf of Chinese Chemical Society and Institute of Materia Medica, Chinese Academy of Medical Sciences.

Lithium-ion batteries (LIBs) have made significant contributions to modern energy storage technologies owing to their long cycle life and environmental friendliness [1–3]. Nevertheless, the uneven distribution and scarcity of lithium resources cannot satisfy the rising market demand, which inevitably hinders its application in large-scale energy storage systems [4,5]. Sodium-ion batteries (SIBs) have emerged and been considered as beneficial complements to LIBs because of abundant sodium resources [6,7]. Unfortunately, the relatively larger radius of Na^+ induces the huge volume change and sluggish electrochemical reaction kinetics, causing the rapid capacity decay and poor fast-charging performance of SIBs [8,9]. Therefore, it is urgent to develop suitable electrode materials with improved electrochemical performance to promote the practical application of SIBs.

At present, various cathode materials have been reported with satisfactory sodium storage performance, including transition metal oxide, polyanion, Prussian blue, and organic materials [10–12]. Noticeably, graphite anode is commonly used in commercial LIBs, but shows a poor sodium storage performance in conventional ester-based electrolyte [13,14]. Inspired by Dahn's pioneering work, hard carbon (HC) anode materials have attracted extensive attention for SIBs due to their unique randomly oriented graphite layers and tunable microstructure [15]. Unfortunately, the practical application of HC is limited by their poor sodium storage capacity and low initial Coulombic efficiency [16,17]. In general, the microstructure of HC is closely related to the electrochemical performance, which is significantly affected by the synthesis conditions [18,19]. Among the reported strategies, pre-oxidation treatment has demonstrated high efficiency in regulating the microstructure of HC for the superior sodium storage performance [20]. However, they mainly concentrate on the improved sodium storage performance of HC, the detailed functional mechanism of pre-oxidation treatment is crucial but ignored. Until now, various precursors have been applied to prepare hard carbon anodes, including brown coal [21], anthracite [22], bituminous coal [23], subbituminous coal [24], pitch [25], *etc.* Among them, brown coal has a significantly lower price than that of anthracite and pitch. Moreover, Yunnan

* Corresponding authors.
E-mail addresses: jiexiao@kust.edu.cn (J. Xiao), linli@wzu.edu.cn (L. Li), zengxiaoyuan@kust.edu.cn (X. Zeng).
[1] These authors contributed equally to this work.

https://doi.org/10.1016/j.cclet.2025.111156
1001-8417/© 2026 Published by Elsevier B.V. on behalf of Chinese Chemical Society and Institute of Materia Medica, Chinese Academy of Medical Sciences.

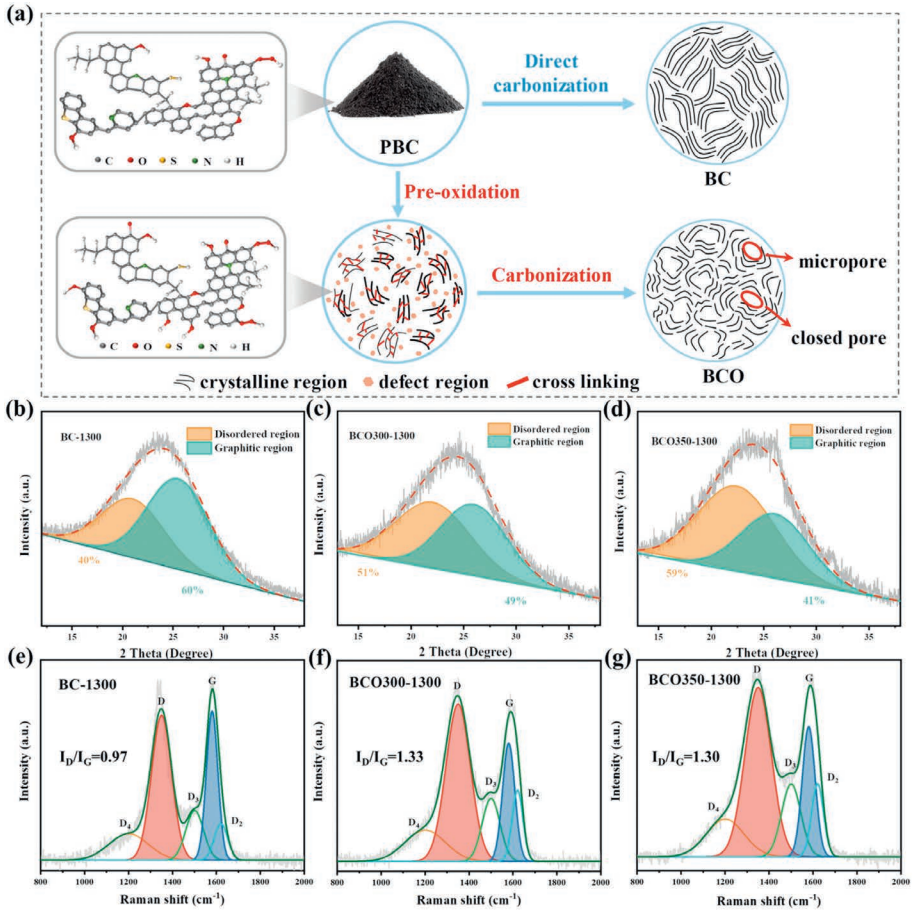


Fig. 1. (a) Schematic illustration of the synthesis process of brown coal-derived HC. (b-d) Fitted XRD spectra, and (e-g) fitted Raman spectra of BC-1300, BCO300-1300 and BCO350-1300, respectively.

Province, situated in the southwestern region of China, represents the most substantial repository of brown coal reserves [26]. Given its abundant availability and low cost, brown coal from Yunnan Province emerges as a promising precursor for the large-scale production of hard carbon materials with high carbon yield.

Herein, brown coal with abundant resources in Yunnan Province is applied as the precursor to prepare HC anode materials for SIBs. The effect of pre-oxidation treatment on the microstructure and electrochemical performance is systematically investigated. The pre-oxidation treatment introduces an abundance of oxygen-containing functional groups with increased disordered phase, which is in favor of the improved sodium storage performance. Therefore, brown coal-derived HC delivers a high reversible specific capacity of 316.1 mAh/g with a high initial Coulombic efficiency of 87.6 %. Moreover, the adsorption-insertion-pore filling sodium storage mechanism is revealed by *in-situ* XRD and Raman.

Brown coal is employed as the precursor due to its low cost and abundant resources in Yunnan Province of China. As illustrated in Fig. 1a, abundant oxygen-containing groups are introduced by the pre-oxidation process, which favors the construction of cross-linking structures and inhibits graphitization degree. The pre-oxidized BCO300 exhibits significantly reduced ash content and enhanced oxygen content in comparison with the pristine brown coal (Table S1 in Supporting information). To investigate the evolution of functional groups in the coal precursors at different pre-oxidation temperatures, Fourier Transform infrared spectroscopy (FTIR) and X-ray photoelectron spectroscopy (XPS) analyses were conducted (Figs. S1 and S2 in Supporting information). The FTIR analysis revealed that oxygen molecules preferentially react with unsaturated functional groups to form oxygen-containing functional groups. The C 1s spectra reveal an obvious increase in the content of C-O, C=O, and C(O)-O functional groups after the pre-oxidation treatment. The thermal stability and carbon yield of the pristine brown coal and BCOX (X = 250, 300 and 350) were investigated by TG-DSC (Fig. S3 in Supporting information). The onset temperature of rapid weight loss in the thermogravimetric (TG) curve of BC is significantly lower than that of BCOX, indicating that pre-oxidation effectively enhances its thermal stability. In addition, the residual mass shows a significant increase, suggesting that pre-oxidation can enhance carbon yield.

The hard carbon from the carbonization of the original brown coal and pre-oxidized brown coal are denoted as BC-1300 and BCOX-1300 (X = 250, 300, and 350), respectively. The effect of pre-oxidation on the structure of HC was firstly investigated by X-ray diffraction (XRD), where the peak fitting of (002) diffraction peak is associated with the proportion of disordered and graphitized regions [27]. As shown in Figs. 1b-d and Fig. S4 (Supporting information), BCOX-1300 shows a higher proportion of disordered regions than BC-1300. Moreover, BCOX-1300 has a larger interlayer spacing than BC-1300, facilitating fast Na^+ diffusion. Subsequently, the Raman spectrum was applied to further disclose the disorder degree of brown coal-derived HC by measuring the intensity ratio of D-band to G-band (I_D/I_G) [28,29]. As shown in Figs. 1e-g and Fig. S5 (Supporting information), the value of I_D/I_G ratio of BC-1300, BCO250-1300, BCO300-1300, and BCO350-1300 are 0.97, 1.19, 1.33, and 1.30, respectively. Moreover, the peak area ratio of A_{D3}/A_G is closely related to the proportion of amorphous carbon and oxygen-containing functional groups, where this value of

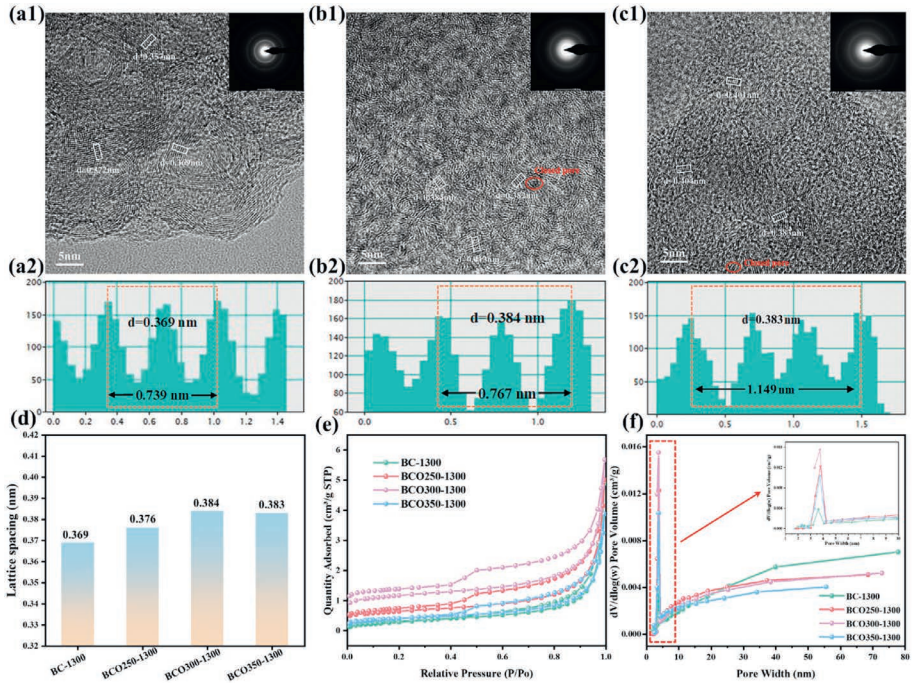


Fig. 2. (a1-c1) HRTEM images and (a2-c2) corresponding fast Fourier transform (FFT) patterns of BC-1300, BCO300-1300 and BCO350-1300, respectively. Insert: SAED patterns of corresponding samples. (d) Lattice spacing, (e) N_2 adsorption-desorption isotherms, and (f) Barrett-Joyner-Halenda (BJH) pore-size distribution curves of BC-1300 and BCOX-1300.

brown coal-derived HC is remarkably increased after pre-oxidation treatment (Table S2 in Supporting information). These indicate that pre-oxidation can effectively inhibit graphitization to obtain increased sodium storage capacity.

The morphologies of brown coal-derived HC are revealed by scanning electron microscopy (SEM) in Fig. S6 (Supporting information). BC-1300 displays a rough and disordered surface morphology. In contrast, smooth surfaces are observed in BCO250-1300 and BCO300-1300 due to the incorporation of oxygen-containing groups during the pre-oxidation process. Subsequently, the microstructure of the brown coal-derived HC was further investigated by high-resolution transmission electron microscopy (HRTEM). As shown in Figs. 2a-c and Fig. S7 (Supporting information), the proportion of disordered microstructure is improved after the pre-oxidation, all BCOX-1300 samples own abundant bent graphite microcrystals and closed nanopores. Meanwhile, the decreased sharpness of dispersing diffraction rings in selected area electron diffraction (SAED) patterns of BCOX-1300 reveals the disordering degree of the local carbon structure is enhanced. Noticeably, the interlayer spacing of brown coal-derived HC is increased with the improved pre-oxidation temperature, the expansion of interlayer spacing is in favor of boosting the sodium storage capacity (Fig. 2d) [30].

The pore characteristics of brown coal-derived HC were disclosed by nitrogen adsorption/desorption isotherms. All of the samples display typical type IV isotherms, indicating the existence of numerous micropores and mesopores (Fig. 2e) [31,32]. As listed in Table S3 (Supporting information), the specific surface area of BC-1300, BCO250-1300, BCO300-1300, and BCO350-1300 are 1.13, 4.04, 1.45 and 2.29 m^2/g, respectively. BCO300-1300 possesses small specific surface area coupled with abundant mesopores (Fig. 2f), which facilitates the diffusion of electrolytes and provides more sodium storage sites. To further characterize the microporous structure, CO_2 adsorption-desorption isotherm measurements were conducted at constant temperature (Fig. S8 in Supporting information). The pore size distribution derived from CO_2 adsorption analysis reveals that all BCOX-1300 samples possess a hierarchical porous architecture, which significantly enhances Na^+ diffusion kinetics. Furthermore, the true density of BCOX-1300 is significantly lower than that of BCO-1300, confirming more closed pores exit in the coal-based hard carbon material after the pre-oxidation treatment (Table S4 in Supporting information). All in all, pre-oxidation treatment plays a key role on the pore structure and microstructure of brown coal-derived HC, which significantly affects the sodium storage performance.

The surface chemical composites of brown coal-derived HC were analyzed by X-ray photoelectron spectroscopy (XPS, Fig. S9 in Supporting information). As shown in Figs. S10a-d (Supporting information), the C 1s spectra of brown coal-derived HC can be deconvoluted into four characteristic peaks of C-C, C-O, C=O and O-C=O. In general, the C-C bond mainly belongs to graphite, while C-O, C=O, and O-C=O bonds belong to the defects of graphite [33]. The proportion of the C-C is significantly decreased, suggesting an improvement in the disorder of BCOX-1300. Subsequently, the increased intensity of C=O in the O 1s spectra of BCOX-1300 further confirms the key role of pre-oxidation treatment (Figs. S10e-h in Supporting information). As indicated in Table S5 (Supporting information), the oxygen content in BCOX-1300 surpasses that in BC-1300, the total oxygen content increases from 4.27 at% to 5.82 at% with the enhancement of pre-oxidation temperature. These results indicate that pre-oxidation treatment can effectively introduce more oxygen-containing functional groups to provide an abundance of active sites for reversible sodium storage.

The superiority of pre-oxidation on electrochemical performance was investigated by assembling Na||HC half cells. As shown in Fig. 3a and Fig. S11 (Supporting information), all the brown coal-derived HC anodes exhibit similar cyclic voltammetry (CV) curves, suggesting the same sodium storage mechanism. Meanwhile, the BCO300-1300 electrode shows a huge potential to obtain a higher reversible capacity due to the maximum peak area. And BCOX-1300 (X = 250, 300 and 350) shows a higher reversible capacity than that of BC-1300 (Fig. 3b). Noticeably, BCO300-1300 delivers the highest reversible capacity of 316.1 mAh/g with a high initial

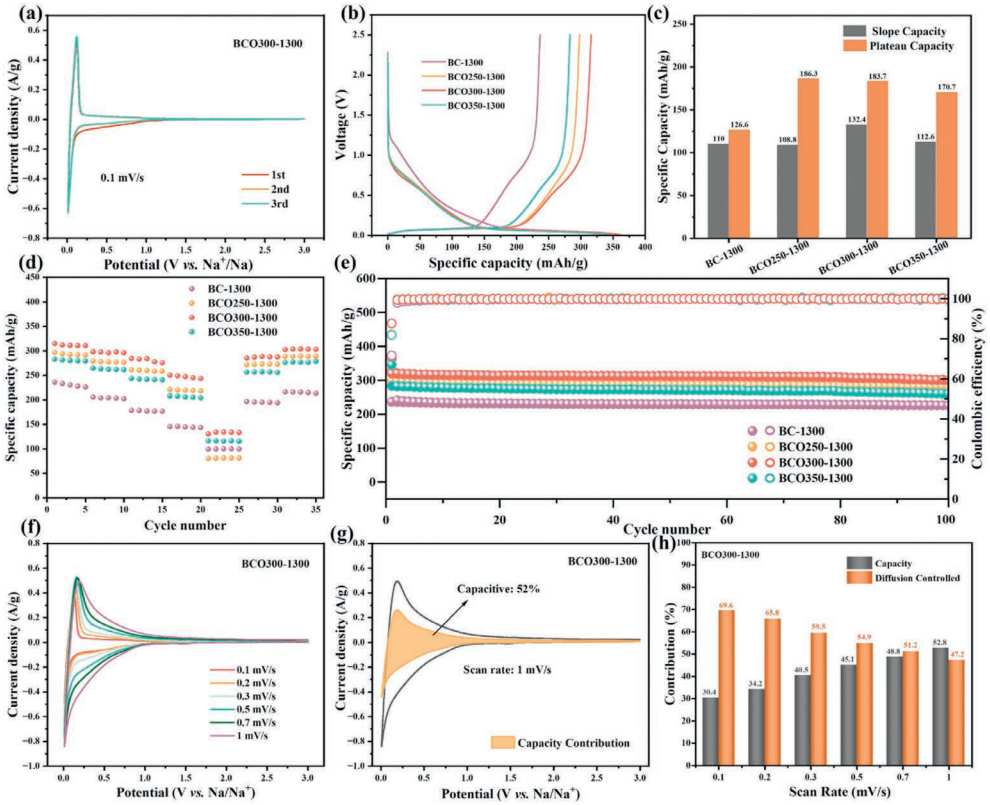


Fig. 3. (a) CV curves of BCO300-1300 at the scan rate of 0.1 mV/s. (b) The initial discharge-charge curves and (c) capacity contribution of the slope region and plateau region in the second discharge curves of BC-1300 and BCOX-1300. (d) Rate performance and (e) cycling performance of BC-1300 and BCOX-1300. (f) CV curves at different scan rates, (g) CV curve at 1 mV/s with shaded region defining pseudo capacitance contribution, and (h) contribution ratios of capacitive and diffusion-controlled processes at various scan rates of BCO300-1300.

Coulombic efficiency of 87.6% (Table S6 in Supporting information). In general, the galvanostatic charge/discharge profiles of the HC anode can be divided into two distinct regions: the high-voltage slope region and low-voltage plateau region. As shown in Fig. 3c, the plateau capacity of BCOX-1300 is significantly higher than that of BC-1300 due to the increased disordered phases and micropore of BCOX-1300 [34]. The rate performance of BC-1300 and BCO300-1300 is estimated in a wide current density from 20 mAh/g to 500 mAh/g. As displayed in Fig. 3d, the rate performance of brown coal-derived HC is greatly improved by pre-oxidation. BCO300-1300 shows a reversible capacity of 315.1, 298.4, 284.8, 250.5 and 130.6 mAh/g at current densities of 20, 50, 100, 200 and 500 mA/g, respectively. A high reversible capacity of 304.7 mAh/g at 20 mA/g is maintained after the evaluation of rate performance, indicating good electrochemical reversibility of BCO300-1300. BCO300-1300 delivers a high reversible capacity of 316.1 mAh/g and capacity retention of 95% after 100 cycles (Fig. 3e). These demonstrate that pre-oxidation is an effective strategy to boost the sodium storage performance of HC.

The sodium storage behavior of BCO300-1300 was further investigated by CV measurements at different scan rates (Fig. 3f). The capacitive and diffusion-controlled contributions of the BCO300-1300 electrode are calculated by [35,36]:

$$i = k_1 v + k_2 v^{1/2} \tag{1}$$

where i, $k_1 v$ and $k_2 v^{1/2}$ are the peak current, capacitive contributions and diffusion-controlled contributions, respectively. As shown in Figs. 3g and h, higher capacitive contributions of BCO300-1300 electrode are observed with the increase of scan rate, which is responsible for the superior rate performance of BCO300-1300 electrode. Subsequently, electrochemical impedance spectroscopy (EIS) measurements were applied to disclose the mechanism of the improved sodium storage performance. As shown in Fig. S12 and Table S7 (Supporting information), the R_{ct} values of BC-1300, BCO250-1300, BCO300-1300, and BCO350-1300 are 10.82, 9.61, 6.98, and 9.03 Ω, respectively. BCO300-1300 electrode shows the lowest R_{ct}, demonstrating its fast electrochemical reaction kinetics.

The Na^+ storage behavior of brown coal-derived HC was further investigated by galvanostatic intermittent titration technique (GITT, Fig. S13 in Supporting information). The diffusion coefficients (D_{Na^+}) of the brown coal-derived HC are calculated based on Fick's second law with the simplified equation [18,37]:

$$D_{Na} = \frac{4}{\pi \tau}\left(\frac{m_b V_m}{M_B A}\right)^2 \left(\frac{\Delta E_S}{\Delta E_\tau}\right)^2 \tag{2}$$

where τ, m_B, V_m, M_B, and A are the pulse duration, active mass of the electrode, molar volume, molecular weight, and active surface area of the electrode, respectively. Additionally, ΔE_S and ΔE_τ are shown in Fig. S14 (Supporting information). A similar change trend of D_{Na^+} is observed in these brown coal-derived HC, demonstrating the similar Na^+ storage behavior (Figs. 4a and b). In general, the lower D_{Na^+} at ~0.6 V is ascribed to the formation of solid electrolyte interface, which limits the diffusion of Na^+ on the surface of brown coal-derived HC. Noticeably, an obvious decrease of D_{Na^+} is observed at 0.1-0.05 V, indicating the slow Na^+ diffusion kinetics between carbon layers. D_{Na^+} increases at 0.05-0.001 V due to the rapid adsorption of Na^+ on the micropores. In the subsequent charging process, the change of D_{Na^+} is almost opposite to the discharge process, which elucidates the highly reversible sodium storage behaviors. In addition, D_{Na^+} between the platform and slope regions of the brown coal-derived HC is illustrated in Fig. S15 (Supporting information). BCO300-1300 exhibits the highest diffusion

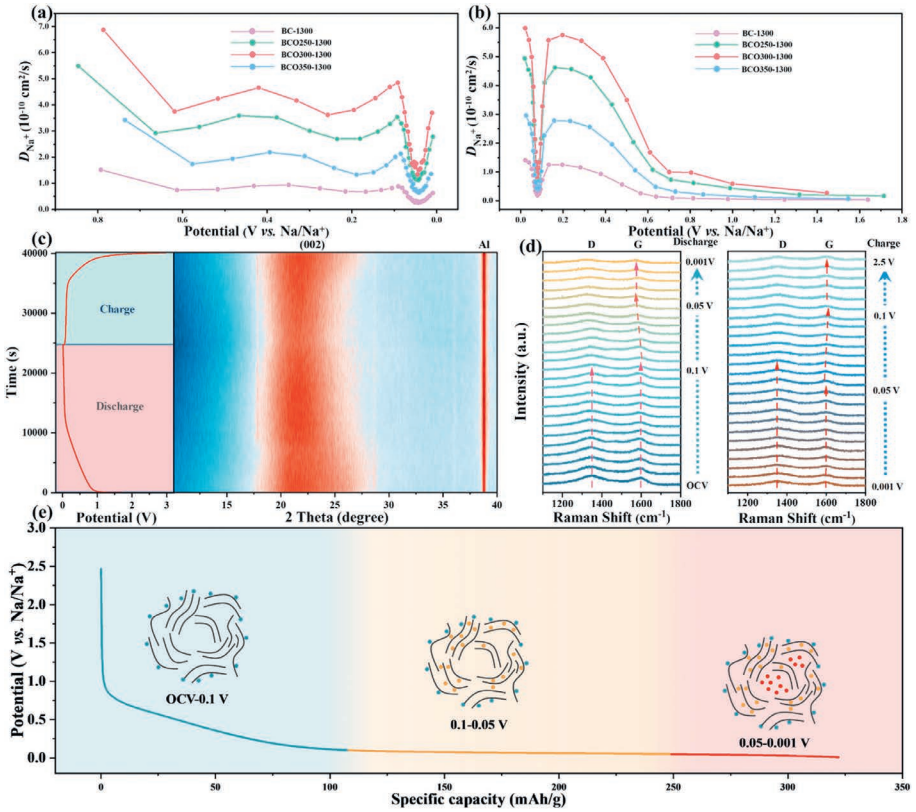


Fig. 4. (a, b) D_{Na^+} of BC-1300, BCO250-1300, BCO300-1300, and BCO350-1300. (c) *In-situ* XRD of BCO300-1300 during the initial cycle. (d) *In-situ* Raman spectroscopy of BCO300-1300. (e) Schematic illustration of sodium storage mechanism of BCO300-1300.

coefficient, demonstrating its fast electrochemical reaction kinetics for superior rate performance.

The structure evolution of BCO300-1300 was investigated by *in-situ* XRD (Fig. 4c). During the discharge process, the position of (002) peak is maintained at the voltage range of >0.1 V, suggesting the surface adsorption of Na^+. The position of (002) peak shifts to a lower angle at 0.1-0.05 V, indicating that Na^+ is intercalated into the carbon layers with an expansion of interlayer spacing. Finally, the position of (002) peak is unchanged when discharged to 0.001 V, revealing the pore-filling behavior of Na^+. The peak change is reversible in the subsequent charging process, which demonstrates the highly reversible sodium storage behaviors for improved cycling stability. Subsequently, *in-situ* Raman spectroscopy was employed to further reveal the structural information of BCO300-1300 during the discharge/charge process (Fig. 4d). The position of D band and G band remains unchanged, and a gradual broadening of D band is detected when discharged to 0.1 V, implying the adsorption of Na^+ on BCO300-1300 surface. At the voltage range of 0.1-0.05 V, an obvious shift of the G-band is observed, confirming the intercalation of Na^+ into the carbon layer. In addition, no significant change of G-band is probed between 0.05 V and 0.001 V (filling of Na^+ on the micropores). In the subsequent charging process, the peaks of D band and G band almost recover to the initial position. As shown in Fig. S16 (Supporting information), the phenolphthalein reagent testing results further demonstrate the highly reversible sodium storage behavior in BCO300-1300 [38,39]. These disclose that the highly reversible sodium storage mechanism of BCO300-1300 is adsorption-insertion-pore filling (Fig. 4e).

In conclusion, a high-performance brown coal-derived HC is synthesized by pre-oxidation treatment. Large amounts of oxygen-containing functional groups are introduced into HC during the pre-oxidation process to regulate its microstructure. The abundant disordered phase in BCO300-1300 facilitates sodium storage, realizing a high reversible specific capacity of 316.1 mAh/g, much higher than that of 236.5 mAh/g in BC-1300. In addition, the highly reversible "adsorption-insertion-pore filling" sodium storage mechanism is demonstrated by *in-situ* XRD and Raman. This work is expected to promote the practical application of pre-oxidation strategy to boost the sodium storage performance of HC for SIBs.

Declaration of competing interest

The authors declare that they have no known competing financial interests or personal relationships that could have appeared to influence the work reported in this paper.

CRediT authorship contribution statement

Ke Liu: Writing – review & editing, Writing – original draft, Investigation, Data curation, Conceptualization. **Yujie Guo:** Investigation. **Boyuan Liu:** Investigation. **Yanjia Zhang:** Investigation. **Yingjie Zhang:** Investigation, Conceptualization. **Xunzhu Zhou:** Writing – review & editing. **Xingqiao Wu:** Writing – review & editing. **Jie Xiao:** Writing – review & editing, Writing – original draft, Supervision, Project administration, Funding acquisition, Conceptualization. **Lin Li:** Writing – review & editing, Writing – original draft, Funding acquisition, Conceptualization. **Xiaoyuan Zeng:** Writing – review & editing, Writing – original draft, Funding acquisition, Conceptualization.

Acknowledgments

This work was supported by the Yunnan Major Scientific and Technological Projects (No. 202202AG050003), the National Natural Science Foundation of China (Nos. 52262034, 52202286), Key Research and Development Program of Zhejiang Province (No.

2024C01057), the Natural Science Foundation of Yunnan Province (No. 202401AW070016), Natural Science Foundation of Zhejiang Province (No. LY24B030006), Key Laboratory of Ionic Rare Earth Resources and Environment, Ministry of Natural Resources of the People's Republic of China (No. 2023IRERE206), Science and Technology Plan Project of Wenzhou Municipality (No. ZG2024055), the Project Funding from "Xingdian Talent Support Plan" and Open Project of Yunnan Precious Metals Laboratory Co., Ltd. (No. YPML-2023050255).

Supplementary materials

Supplementary material associated with this article can be found, in the online version, at doi:10.1016/j.cclet.2025.111156.

References

[1] H. Kim, J.C. Hyun, D.H. Kim, et al., Adv. Mater. 35 (2023) 2209128.
[2] Z. Fan, X. Zhou, J. Qiu, et al., Angew. Chem. Int. Ed. 62 (2023) e202308888.
[3] X.T. Li, J. Chou, Y.H. Zhu, et al., eScience 3 (2023) 100121.
[4] C. Vaalma, D. Buchholz, M. Weil, S. Passerini, Nat. Rev. Mater. 3 (2018) 1–11.
[5] M. Hadouchi, J. Hou, T. Koketsu, A. Lahmar, J. Ma, Nano Res. 17 (2024) 1427–1440.
[6] S. Lee, G. Kwon, K. Ku, et al., Adv. Mater. 30 (2018) 1704682.
[7] J. Chen, Z. Yang, X. Xu, et al., Adv. Mater. 36 (2024) 2400169.
[8] D.A. Stevens, J.R. Dahn, J. Electrochem. Soc. 148 (2001) A803.
[9] E. Gabriel, C. Ma, K. Graff, et al., eScience 3 (2023) 100139.
[10] X. Pu, H. Wang, D. Zhao, et al., Small 15 (2019) 1805427.
[11] Z. Hao, X. Shi, W. Zhu, et al., ACS Nano 18 (2024) 9354–9364.
[12] C. Zheng, S. He, J. Gan, et al., Carbon Energy (2024) e605.
[13] J.M. Cao, K.Y. Zhang, J.L. Yang, et al., Chin. Chem. Lett. 35 (2024) 109304.
[14] K.Y. Zhang, Y.Q. Fu, H.H. Liu, et al., Phys. Scr. 98 (2023) 125977.
[15] D.A. Stevens, J.R. Dahn, J. Electrochem. Soc. 147 (2000) 1271.
[16] P. Wang, Y.J. Guo, W.P. Chen, et al., Nano Res. 16 (2023) 3832–3838.
[17] Y. Yang, C. Wu, X. He, et al., Adv. Funct. Mater. 34 (2024) 2302277.
[18] A. Gomez-Martin, J. Martinez-Fernandez, M. Ruttert, et al., Chem. Mater. 31 (2019) 7288–7299.
[19] H. Mao, S. Yang, Y. Yang, et al., Carbon Neutralization 3 (2024) 673–688.
[20] Y. Lu, C. Zhao, X. Qi, et al., Adv. Energy Mater. 8 (2018) 1800108.
[21] Y. Zou, H. Li, K. Qin, et al., J. Mater. Sci. 55 (2020) 5994–6004.
[22] Y. Dong, S. Yuan, W. Zhao, et al., J. Mater. Chem. A 11 (2023) 9668–9681.
[23] Q.Q. Tian, X.M. Li, L.J. Xie, et al., New Carbon Mater. 38 (2023) 939–953.
[24] H. Lu, S. Sun, L. Xiao, et al., ACS Appl. Energy Mater. 2 (2019) 729–735.
[25] J. Wang, L. Yan, B. Liu, et al., Chin. Chem. Lett. 34 (2023) 107526.
[26] Q. Zhao, Clean Coal Technol. 24 (2018) 9–14.
[27] Y. Chen, H. Sun, X. He, et al., Small 20 (2023) 2307132.
[28] R. Xu, Z. Yi, M. Song, et al., Carbon 206 (2023) 94–104.
[29] L. Wang, Z. Xu, P. Lin, et al., Adv. Energy Mater. 15 (2025) 2403084.
[30] X. Yin, Z. Lu, J. Wang, et al., Adv. Mater. 34 (2022) 2109282.
[31] R. Wang, J.M. Lee, S. Khoshk Rish, et al., Fuel Process. Technol. 238 (2022) 107498.
[32] B. Xing, H. Zeng, G. Huang, et al., Electrochim. Acta 376 (2021) 138043.
[33] Y. Zhang, X. Li, P. Dong, et al., ACS Appl. Mater. Interfaces 10 (2018) 42796–42803.
[34] G. Zhao, T. Xu, Y. Zhao, et al., Energy Storage Mater. 67 (2024) 103282.
[35] R.C. Cui, B. Xu, H.J. Dong, C.C. Yang, Q. Jiang, Adv. Sci. 7 (2020) 1902547.
[36] C. Lin, J. Zhang, Y.V. Lim, et al., Carbon Neutralization 1 (2022) 224–232.
[37] M.Y. Su, K.Y. Zhang, E.H. Ang, et al., Rare Metals 43 (2024) 2585–2596.
[38] S. You, Q. Zhang, J. Liu, et al., Energy Environ. Sci. 17 (2024) 8189–8197.
[39] Z. Wang, X. Feng, Y. Bai, et al., Adv. Energy Mater. 11 (2021) 2003854.